PCCP

ROYAL SOCIETY OF CHEMISTRY

PAPER

View Article Online
View Journal | View Issue



Cite this: *Phys. Chem. Chem. Phys.*, 2026, **28**, 3282

# Carbon vacancy network mediated hydrogen trapping at the α-Fe/VC interface

Linxian Li,[a] Huifang Lan,[a] Shuai Tang,*[a] Fengliang Tan,[b] Qing Peng,*[cd] Zhenyu Liu[a] and Guodong Wang[a]

Hydrogen embrittlement poses a significant threat to the structural integrity of high-strength steels. Although vanadium carbide (VC) precipitates are recognized as effective traps for mitigating hydrogen-induced damage, the precise mechanisms of hydrogen trapping and diffusion within VC remain controversial. In this study, we employ first-principles calculations to investigate the influence of carbon vacancies on hydrogen trapping and diffusion behavior at the coherent α-Fe/VC interface. Our results reveal that interfacial carbon vacancies facilitate hydrogen approach along the *xy*-plane, while interconnected vacancy networks enable hydrogen to diffuse from the α-Fe matrix into the VC bulk. Notably, hydrogen ingress into VC occurs preferentially through nearest-neighbor carbon vacancies. The calculated activation energies for hydrogen escape from interfacial and internal VC vacancies are 67.5 kJ mol$^{-1}$ and 82.2–83.9 kJ mol$^{-1}$, respectively, in good agreement with experimental values. These findings underscore the critical role of interfacial and connected carbon vacancies in mediating hydrogen diffusion and trapping within VC, providing atomistic insights for designing hydrogen-resistant steels.

Received 5th November 2025,
Accepted 15th December 2025

DOI: 10.1039/d5cp04264j

rsc.li/pccp



## 1. Introduction

High-strength steels are crucial in industries such as automotive manufacturing and aerospace due to their exceptional mechanical properties and cost-effectiveness.[1–5] However, their service life is often compromised by the notorious hydrogen embrittlement, a phenomenon where the structural integrity of metals is degraded after absorbing hydrogen.[6,7] As a result, reducing the hydrogen embrittlement susceptibility of steel has become a significant research focus. Although no single mechanism can comprehensively account for all facets of hydrogen embrittlement, it is widely accepted that the accumulation of diffusely distributed hydrogen atoms at lattice defects plays a key role in causing hydrogen embrittlement.[8–10] Consequently, incorporating irreversible hydrogen traps into the material can help prevent the aggregation of hydrogen atoms, thereby improving resistance to hydrogen embrittlement.[11–15]

Carbides play a crucial role in mitigating hydrogen embrittlement while enhancing the strength of steel, with vanadium carbide (VC) being particularly noteworthy due to its relatively low cost and favorable formation energy.[16–20] Both experimental and theoretical studies have demonstrated that due to the presence of numerous carbon (C) vacancies in VC precipitates,[21–23] VC has the ability to trap a significant amount of diffused hydrogen atoms, thereby effectively reducing the risk of hydrogen embrittlement in steels.[24,25] Experimental observations typically show that VC precipitates have a discoidal shape, with a B–N orientation relationship with the matrix ($(001)_{Fe}//(001)_{VC}$, $[100]_{Fe}//[110]_{VC}$). The hydrogen trapping capacity of VC carbides peaks at around 10 nm in size.[26] For instance, Yang *et al.* found that VC precipitates could decrease the hydrogen embrittlement susceptibility of spring steels by 23%.[27] Additionally, Boot *et al.* measured the hydrogen activation energy of VC precipitates to be between 53 and 72 kJ mol$^{-1}$ using thermal desorption spectroscopy (TDS) experiments, suggesting that VC acts as an irreversible hydrogen trap.[28] The specific sites where hydrogen is trapped within VC have also been extensively studied. Takahashi *et al.*[29] identified C vacancies at the interface between the V4C3 precipitate phase and the matrix as primary hydrogen trapping sites using atom probe tomography (APT). In contrast, Chen *et al.*[30] revealed through low-temperature APT experiments that hydrogen can be trapped inside VC precipitates. Certain researchers have indicated that hydrogen diffusion into the interior of carbides requires a continuous network of carbon vacancies within the lattice.[31,32] While the hydrogen trapping properties of VC precipitates are well-known, the processes governing hydrogen diffusion near the interface and its entry into the interior of the carbide

[a] *State Key Laboratory of Digital Steel, Northeastern University, Shenyang 110819, China*
[b] *School of Materials and Environmental Engineering, Hunan University of Humanities, Science and Technology, Loudi 417000, China*
[c] *School of Power and Mechanical Engineering, Wuhan University, Wuhan 430072, China*
[d] *Xinyan Semi Technology Co. Ltd, Wuhan, 430075, China*

are not yet fully understood. A clear understanding of hydrogen trapping and diffusion both perpendicular and parallel to the interface is still missing.

First-principles calculations have been widely used to evaluate the hydrogen trapping and diffusion capacities of various materials, providing insights into the intrinsic mechanisms. Ma *et al.*[33] suggested that strain at the carbide interface enhances hydrogen trapping at specific sites. Zhang *et al.*[34] found that the hydrogen trapping energy at the interface can be correlated with the Bader atomic volume. Stefano *et al.*[15] calculated the hydrogen escape energies at different trapping sites of Ti precipitates in steel, and found that these energies were well contrasted with the experimental results. Sagar *et al.*[35] indicated that C vacancies at the α-Fe/TiC interface act as deep hydrogen traps, and that hydrogen diffusion through the interface to these C vacancies is feasible. However, previous studies have primarily focused on whether hydrogen atoms can penetrate the interface and diffuse into the interfacial C vacancies, without providing a detailed analysis of the role that C vacancies play in this process. This also involves the hydrogen trapping and diffusion behavior of hydrogen atoms both perpendicular and parallel to the interface. Furthermore, previous studies have not provided a detailed explanation of the physical representation of hydrogen trapping inside the carbide, as observed through APT. Therefore, further investigation is needed into how hydrogen is captured and migrates within the VC region of the interface. This is crucial for optimizing the hydrogen trapping ability of vanadium carbide.

In this study, first-principles calculations are employed to explore hydrogen trapping sites at the coherent α-Fe/VC interface, considering both the presence and absence of C vacancies. Then, the diffusion behavior of hydrogen perpendicular and parallel to the interface is explored. Finally, the diffusion of hydrogen within the VC layer near the interface is analyzed to elucidate the mechanisms of hydrogen trapping and diffusion by VC precipitates.

## 2. Theoretical methods

The Vienna *Ab initio* Simulation Package (VASP)[36] was used to perform first-principles calculations based on density functional theory (DFT). The electron–ion interactions are described using the projector augmented wave (PAW) method.[37] The Perdew–Burke–Ernzerhof (PBE) functional[38] within the generalized gradient approximation (GGA)[39] is used to approximate the exchange–correlation effects. All calculations were performed using a plane-wave cutoff energy of 450 eV. A model of the α-Fe/VC coherent interface, consisting of 12 layers of VC and 8 layers of Fe, was constructed based on the experimentally determined Baker–Nutting (B–N) orientation to approximate the exchange–correlation effects. All calculations were performed using a plane-wave cutoff energy of 450 eV. A model of the α-Fe/VC coherent interface, consisting of 12 layers of VC and 8 layers of Fe, was constructed based on the experimentally determined Baker–Nutting (B–N) orientation relationship, with $(001)_{Fe}//(001)_{VC}$ and $[100]_{Fe}//[110]_{VC}$.[12,40,41] Previous studies[25,42,43] have indicated that the lowest interfacial energy is achieved when Fe atoms align with C atoms at the α-Fe/VC coherent interface, so this configuration was used. For the initial interface model, the atomic positions and cell size were relaxed, while in subsequent calculations, only the atomic positions were relaxed. The force and energy convergence thresholds were set to 0.01 eV Å$^{-1}$ and $10^{-5}$ eV per cell, respectively. The Brillouin zone of the interface model was sampled using a $6 \times 6 \times 1$ $k$-point grid, constructed based on the Monkhorst–Pack method.[44] Spin-polarized calculations were performed to explain the ferromagnetism of α-Fe. The climbing image nudged elastic band (CINEB) method was used to calculate the hydrogen diffusion energy barrier at the interface.[45] The crystal structures were visualized with the help of VESTA software.[46] Furthermore, to facilitate comparison with experimental values in the literature, the conversion relation 1 eV = 96.49 kJ mol$^{-1}$ is adopted throughout this work.

The vacancy formation energy is defined as the ease of formation of the $n$th C vacancy near the α-Fe/VC coherent interface, which is defined as:

$$E_f^{n\mathrm{Vac}} = E_{n\mathrm{Vac}} + \mu_C - E_{(n-1)\mathrm{Vac}} \quad (1)$$

where $E_{n\mathrm{Vac}}$ refers to the system energy with $n$ carbon vacancies, while $\mu_C$ represents the chemical potential of carbon, calculated based on the average energy per carbon atom in graphite. A negative value for the vacancy formation energy indicates that the formation of the vacancy is energetically favorable.

The segregation energy denotes the energy difference required for a H atom to migrate from the most stable interstitial site within the bulk α-Fe matrix to a specific site at the interface. It is defined as:

$$E_{seg} = (E_{tot}n\mathrm{H} - E_{tot}(n-1)\mathrm{H}) - (E_{tot}^{Fe}(\mathrm{H}) - E_{tot}^{Fe}(\mathrm{O})) \quad (2)$$

where $E_{tot}n$H represents the system energy with $n$ hydrogen atom at the interface. $E_{tot}^{Fe}$(H) represents the energy of the α-Fe matrix with a hydrogen atom in its most stable site, while $E_{tot}^{Fe}$(O) is the energy of the α-Fe matrix without hydrogen atoms. A negative segregation energy indicates that hydrogen atoms tend to segregate to this site.

## 3. Results and discussion

### 3.1. Hydrogen trapping at the α-Fe/VC interface

The α-Fe/VC interface model was initially constructed, considering both C vacancy-free and C vacancy-containing configurations, as illustrated in Fig. 1(a)–(d). The vacancy configurations examined include a single C vacancy ($Vac_C^{int}$), double C vacancies ($Vac_C^{int}$, $Vac_C^{1NN}$), and triple C vacancies ($Vac_C^{int}$, $Vac_C^{1NN}$, $Vac_C^{2NN}$). The double C vacancy configuration is obtained by introducing a nearest neighbor C vacancy on the second VC layer, based on the single C vacancy configuration, as previous studies have hypothesized that hydrogen in carbides can diffuse through connected C vacancies.[32,47] Based on the optimized double carbon vacancy configuration, all possible carbon vacancies on the third layer of VC that satisfy the nearest neighbor condition relative to existing

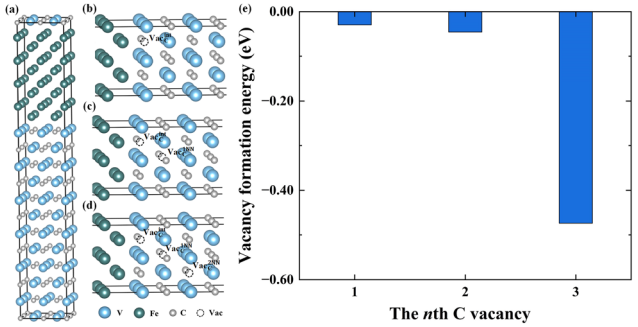


Fig. 1 Four interfacial configurations and corresponding vacancy formation energies: (a) C vacancy-free, (b) single C vacancy, (c) double C vacancy, and (d) triple C vacancy configurations; and (e) the corresponding vacancy formation energies.

vacancies were screened. Each candidate structure was optimized, and the configuration with the lowest total energy was selected as the stable triple vacancy state for subsequent analysis. Fig. 1(e) shows the vacancy formation energies for these configurations. The results show that the vacancy formation energies for all three vacancy configurations are negative, suggesting that these configurations are readily formed and energetically favorable.

To investigate the trapping of individual hydrogen atoms near the α-Fe/VC coherent interface, five types of hydrogen trapping sites were considered as displayed in Fig. 2a: two tetrahedral interstitial sites ($Tet_{Fe}^{nNN}$ and $Tet_{Fe}^{int}$, positioned at the core of four metal atoms), two C vacancies ($Vac_C^{nNN}$ and $Vac_C^{int}$, positioned at the core of six metal atoms), and one triangular interstitial site ($Tri_v$, positioned at the core of three V atoms). The superscript "int" denotes sites at the interface, while "*n*NN" indicates sites relative to the *n*th nearest neighbour to the interface plane. Among them, the tetrahedral interstitial and triangular interstitial are the most stable trapping sites in the defect-free bulk phases of Fe and VC, respectively.[48,49] The trapping configurations and corresponding segregation energies are displayed in Fig. 2. The results show that, without C vacancies, hydrogen atoms tend to segregate to the tetrahedral interstitial site in the Fe layer near the interface. However, due to the positive segregation energy of the triangular interstitial site in the VC layer, hydrogen atoms are unable to segregate to the VC side of the interface when C vacancies are absent. When C vacancies are present, the segregation energy of the trapping

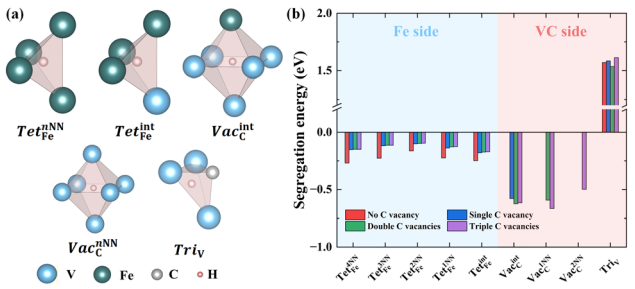


Fig. 2 (a) Different hydrogen trapping sites and (b) the corresponding segregation energies near the interface.

sites near the Fe layer at the interface increases but remains negative, indicating that hydrogen atoms still tend to segregate to these sites. Although interfacial vacancies significantly reduce the segregation energies of adjacent iron layers, the addition of further vacancies within VC (*e.g.*, double or triple vacancy configurations) scarcely alters these segregation energies. Therefore, only the C vacancies closest to the interface significantly affect hydrogen trapping in the Fe layer. Additionally, C vacancies exhibit the strongest trapping ability among all the sites, with all three configurations acting as strong hydrogen traps. Conversely, the triangular interstitial site on the VC side remains ineffective in trapping hydrogen atoms. Therefore, it can be concluded that only C vacancies serve as stable hydrogen trapping sites in carbides within steel.

### 3.2. Hydrogen diffusion at the α-Fe/VC interface

The mobility of hydrogen atoms towards the trapping site is essential for hydrogen trapping and embrittlement mitigation. To that end, we have examined the diffusion behavior of hydrogen atoms near the interface. The diffusion of hydrogen in the *Z* direction (perpendicular to the interface) was scrutinized firstly. The diffusion pathways and corresponding energy barriers for hydrogen atoms in different interface configurations are shown in Fig. 3. Without C vacancies, the diffusion energy barrier for hydrogen near the interface is similar to that in the Fe matrix ($E_{mig}^{Fe}$ = 0.09 eV),[50,51] allowing hydrogen atoms to diffuse near the interface. For various hydrogen traps within steel, extensive literature has determined their corresponding activation energies *via* TDS testing. The activation energies for most traps fall within 100 kJ mol$^{-1}$.[52–54] Only TiC exhibits a significantly higher activation energy, reaching 145 kJ mol$^{-1}$.[55] Conversely, the energy barrier for hydrogen atoms diffusing through the interface into the VC layer is exceptionally high (2.14 eV, 206.5 kJ mol$^{-1}$), which significantly impedes hydrogen diffusion into the VC layer. Thus, considering both the segregation energy and diffusion behavior inferred that hydrogen is likely to remain within the Fe layer when no C vacancy is present.

In contrast, when a C vacancy is present at the interface, hydrogen can still diffuse into the Fe layer, and the energy barrier for the hydrogen atom to pass through the interface and occupy a C vacancy in the VC layer is only 0.30 eV. This allows hydrogen atoms to diffuse into the interface and become trapped by C vacancies. The interfacial vacancy-induced barrier (0.30 eV) is 85% lower than the defect-free case (2.14 eV), demonstrating vacancy-mediated hydrogen permeation. However, the diffusion energy barrier remains high (>2.39 eV) for hydrogen atoms attempting to move from these C vacancies to the triangular interstitial sites within VC. This high barrier prevents hydrogen atoms trapped by the C vacancy from escaping into the defect-free region of VC. When connected C vacancies exist in the VC layer near the interface, the diffusion energy barrier decreases to around 0.82–0.89 eV. This substantial reduction in energy barrier increases the likelihood of hydrogen atoms being trapped within the interior of the carbide.

 

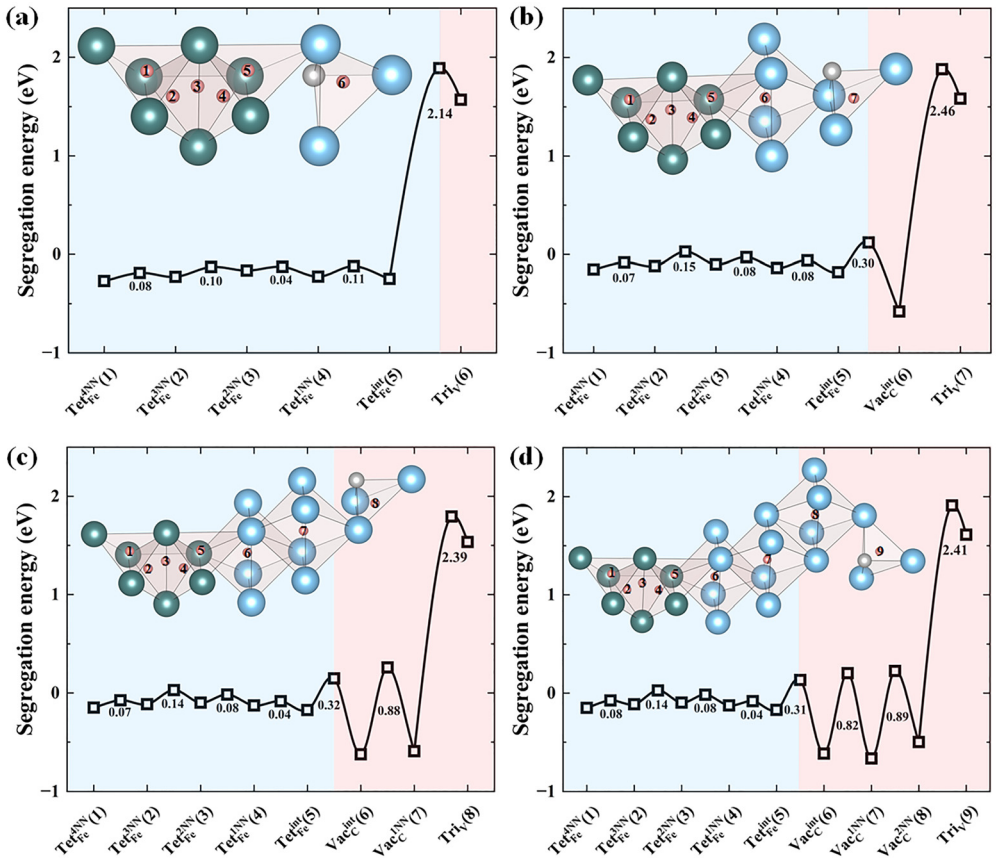


Fig. 3 Hydrogen diffusion paths and energy barriers for different interfaces: (a) C vacancy-free, (b) single C vacancy, (c) double C vacancies, and (d) triple C vacancies.

Additionally, TDS has been widely employed to measure the activation energy of hydrogen traps,[56–58] which refers to the energy needed for hydrogen to escape from a trap. In this study, this activation energy corresponds to the maximum diffusion energy barrier that a hydrogen atom must overcome to migrate from various hydrogen trap sites into the Fe matrix. Based on the data in Fig. 3, the diffusion energy barriers for hydrogen atoms from different sites to the matrix have been calculated (maximum energy barriers required for diffusion from the site on the right to the site on the left in each picture of Fig. 3), with the results summarized in Table 1. In this context, the C-vacancy-free configuration represents the trapping capacity on the Fe side of the interface, the single C vacancy configuration corresponds to the ability of the C vacancy at the interface to trap hydrogen, and the double and triple C vacancy configurations define the trapping capacity within the carbide. The calculated activation energy of hydrogen in the interfacial Fe layer is 12.4 kJ mol$^{-1}$. It is important to note that the interface creates strain on the Fe side. However, due to the model size limitation, a strictly strain-free Fe bulk phase is not included in the calculations, leading to an error in calculating the activation energy on the Fe side of the interface. To estimate the activation energy on the Fe side, the formula proposed in the literature ($E_{act} = E_{seg} + E_{mig}^{Fe}$) can be applied,[15,25,59] giving an activation energy range of 24.5–34.7 kJ mol$^{-1}$. The hydrogen activation energy in grain boundaries and dislocations is generally reported to be in the range of 14.5–18.9 kJ mol$^{-1}$,[60–62] which is categorized as a reversible hydrogen trap at room temperature (<50 kJ mol$^{-1}$ (ref. 63 and 64)). Therefore, the trapping sites on the Fe side of the interface can also be regarded as reversible hydrogen traps, from which hydrogen can escape. The activation energy on the Fe side of the interface

Table 1 Calculated and experimental values of hydrogen escape at different sites of the VC/α-Fe interface

| | Interface | | Interior of the carbide | |
|---|---|---|---|---|
| Site | Fe side | C vacancy on the interface | Double C vacancies | Triple C vacancies |
| This work (kJ mol$^{-1}$) | 24.5–34.7 | 67.5 | 82.2 | 83.9 |
| Experiment (kJ mol$^{-1}$) | 19.8–29.8,[29] 26.8,[29] 33–35[65] | 62–65,[17] 49.6–69.6,[29] 62[67] | 62–82,[28] 87.3[66] | |

is close to the TDS results reported in the literature (19.8–29.8 kJ mol$^{-1}$,[29] 26.8 kJ mol$^{-1}$,[18] 33–35 kJ mol$^{-1}$ (ref. 65)). The fact that APT results did not detect hydrogen trapping at the interface could be attributed to the lack of low-temperature APT, as the hydrogen might have already escaped from the trapping sites by the time of detection.

For the trapping sites in the VC layer, the activation energy obtained by the equation is lower than the calculated value from CINEB. Thus, the activation energies for interfacial C vacancies and internal C vacancies in carbides are determined using CINEB. The calculated escape energies for hydrogen at the interfacial C vacancies and within the carbides are 67.5 kJ mol$^{-1}$ and 82.2–83.9 kJ mol$^{-1}$, respectively. This indicates that both interfacial and internal C vacancies in carbides act as irreversible hydrogen traps, significantly reducing the susceptibility of steel to hydrogen embrittlement.[27] These values are close to the activation energies obtained by TDS,[17,28,29,66,67] and the presence of hydrogen trapping at interfacial C vacancies and within carbides has been confirmed by characterization techniques such as atomic force microscopy (AFM), APT and secondary ion mass spectrometry (SIMS). The synergy between interfacial and connected bulk vacancies creates a "vacancy highway" for hydrogen diffusion, explaining the high hydrogen retention observed in APT studies. The computational results presented here further substantiate the potential for hydrogen trapping within carbide phases and offer a valuable reference for future TDS experiments aimed at verifying hydrogen trapping sites.

The diffusion of hydrogen atoms within the *xy*-plane of the interface was analyzed to understand the impact of the interface and the presence of C vacancies on hydrogen diffusion. The study focused on the five Fe layers closest to the interface, with the diffusion paths and corresponding energy barriers illustrated in Fig. 4. When C vacancies are absent, the diffusion energy barrier for the hydrogen atom is the lowest within the first two layers adjacent to the interface. This suggests that when hydrogen diffuses toward the VC/α-Fe interface, it preferentially migrates along the *z*-axis (perpendicular to the interface) toward the interface, followed by diffusion within the *xy* plane (parallel to the interface) in these two closest layers. When C vacancies are introduced, the diffusion energy barrier for the hydrogen atom in the two layers closest to the interface is further lowered, while it increases in the remaining three layers. As a result, even if there is no C vacancy directly beneath the hydrogen moving from the Fe matrix to the interface, the hydrogen is attracted by the nearby C vacancy, causing the hydrogen atom to diffuse along the *xy*-plane of the interface toward the C vacancy. As the hydrogen atoms move towards these vacancies, they can eventually break through the interface and become trapped within the C vacancies. The process continues until all available vacancies at the interface are filled.

Additionally, the possibility of hydrogen diffusion in the Fe layer toward the second-layer C vacancy ($Vac_C^{1NN}$) near the interface, in the absence of an interfacial C vacancy ($Vac_C^{int}$), was considered. The results are shown in Fig. 5. The vacancy formation energy for $Vac_C^{1NN}$ is −0.24 eV, indicating that this configuration is energetically favorable. The diffusion energy barrier for a hydrogen atom moving from the $Tet_{Fe}^{int}$ site in the Fe layer to the $Vac_C^{1NN}$ site in the VC layer was then calculated. The diffusion energy barrier for hydrogen *via* this pathway to the VC layer is quite high (2.15 eV), which is similar to the diffusion barrier without C vacancies. This result suggests that hydrogen atoms have difficulty in diffusing through this pathway to reach and be trapped by the C vacancies within the VC layer. These findings emphasize the importance of interfacial C vacancies: without them, even if numerous C vacancies exist inside VC, VC cannot act as an irreversible hydrogen trap, as hydrogen atoms struggle to penetrate the interface and reach the deeper hydrogen traps.

### 3.3. Hydrogen diffusion in the interfacial VC layer

The case of diffusion of hydrogen occupying the interfacial C vacancies through the C vacancies located at the second and third nearest neighbors (cross-layer diffusion) was also

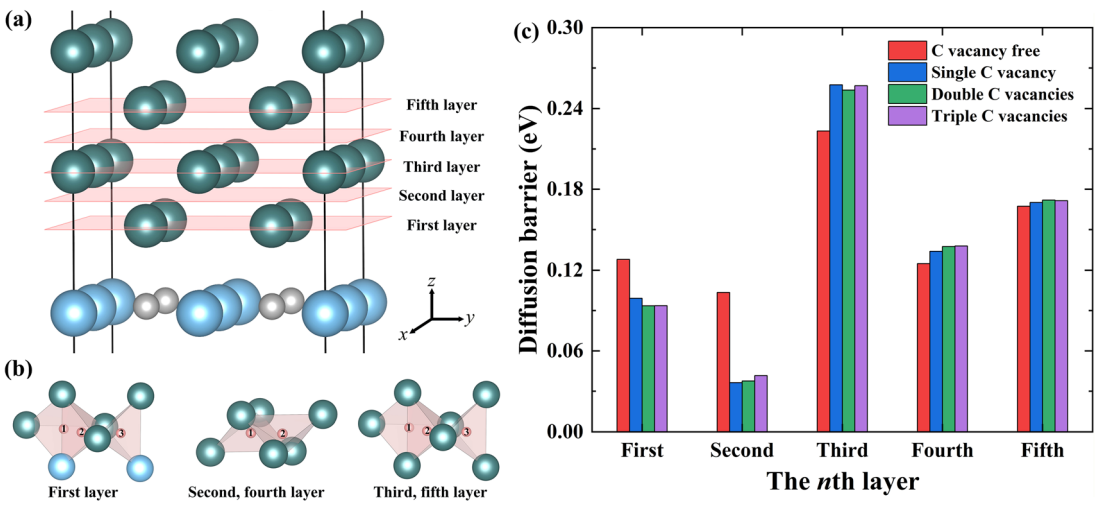


Fig. 4 Hydrogen diffusion paths and energy barriers on the *xy*-plane of the interface. (a) Schematic of diffusion, (b) diffusion paths, and (c) diffusion energy barriers.

 

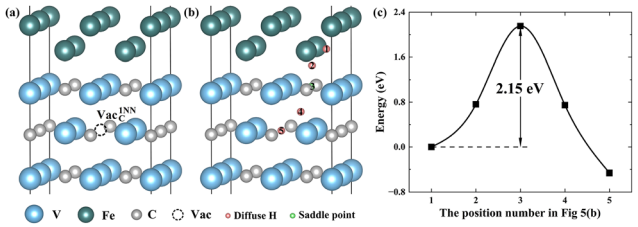


Fig. 5 Formation energy and hydrogen diffusion of the $Vac_C^{1NN}$ configuration. (a) Formation energy of the $Vac_C^{1NN}$ configuration; (b) path of hydrogen diffusion into the $Vac_C^{1NN}$ site, and (c) energy barrier of hydrogen diffusion into the $Vac_C^{1NN}$ site.

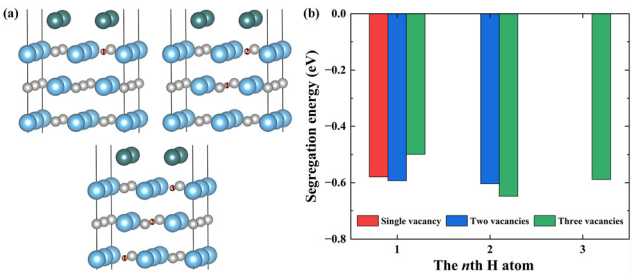


Fig. 7 Multi-hydrogen trapping at C vacancies at the interface. (a1)–(a3) Trapping sites and (b) segregation energy.

considered, and the results are shown in Fig. 6. The formation energies of the second and third nearest neighbor C vacancies were −0.11 eV and −0.77 eV, respectively. These results indicate that both vacancy configurations are energetically feasible. However, the diffusion energy barriers for hydrogen atoms through these second and third nearest neighbor C vacancies (3.56 eV and 2.58 eV) are much larger than the energy barriers for diffusion through the nearest neighbor C vacancies directly connected to the interface. Therefore, the hydrogen atoms in the VC layer at the interface are more inclined to diffuse into the interior of the carbide through the connected C vacancies between neighboring layers, making cross-layer diffusion difficult to occur.

The trapping ability of the interfacial C vacancies also merits further exploration, which is related to the number of hydrogen atoms that can be captured by the C vacancies. Therefore, the ability of three different C vacancy configurations to trap multiple hydrogen atoms was examined, and the findings are shown in Fig. 7. It can be found that even as the number of trapped hydrogen atoms increases, the segregation energy at any C vacancy remains low ($<-0.5$ eV). This indicates that the hydrogen atoms occupying the C vacancies have little effect on the trapping capacity of the adjacent C vacancies. Therefore, under favorable conditions, hydrogen atoms are energetically inclined to occupy all C vacancies in VC.

Besides single hydrogen atom diffusion, we have examined the diffusion of multiple hydrogen atoms within the interfacial VC layer, focusing on diffusion along the network of C vacancies. We have used a model with the three C vacancy configuration and examined two potential diffusion paths. The first path involves hydrogen diffusion through the C vacancies that are directly connected as nearest neighbors. In this path, only after the first hydrogen atom diffuses into the interior of VC through the nearest neighbor C vacancy, the second hydrogen atom can diffuse into the interior of VC in the same manner. The second diffusion path considers the hydrogen atom bypassing the hydrogen atom occupying the nearest neighbor C vacancy and directly diffusing to the third nearest neighboring C vacancy. The schematic diagrams of these two diffusion paths and their respective energy barriers are presented in Fig. 8. The energy barrier for the first diffusion pathway is 0.87 eV, whereas the second path shows a barrier of 1.57 eV. This indicates that hydrogen atoms are more likely to diffuse sequentially into the VC interior *via* the nearest neighbor connected C vacancies. The energy barrier for the first path aligns with experimental values obtained by TDS,[17,66,67] supporting the feasibility of this diffusion process. Therefore, hydrogen atoms diffusing from the α-Fe matrix into the VC layer can only enter the interior of vanadium carbide through the nearest neighboring carbon vacancies. The subsequent hydrogen atom can follow the same diffusion path only after the previous one has diffused into the VC interior.

### 3.4. Effect of C vacancies on hydrogen diffusion at the interface

Based on the computational data presented in this paper, a schematic diagram of hydrogen diffusion near the α-Fe/VC interface with and without C vacancies is constructed, as shown in Fig. 9. When no C vacancies are present in VC, the Fe layers

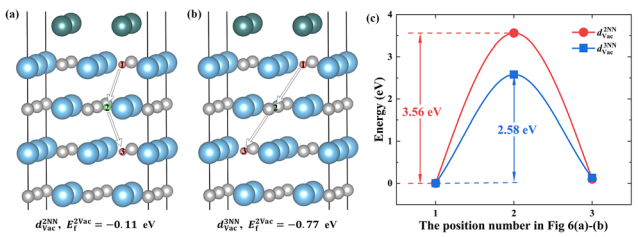


Fig. 6 Paths and energy barriers for hydrogen atom diffusion through other near neighbor C vacancies. (a) Paths of hydrogen diffusion between the second nearest neighbor C vacancies, (b) paths of hydrogen diffusion between the third nearest neighbor C vacancies, and (c) diffusion energy barriers corresponding to different paths.

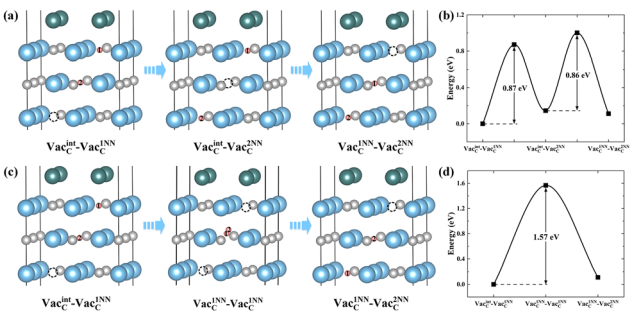


Fig. 8 Multi-hydrogen diffusion in the C vacancy at the interface. The first (a) and second (c) diffusion pathways, and the diffusion energy barriers for the first (b) and second (d) diffusion paths.

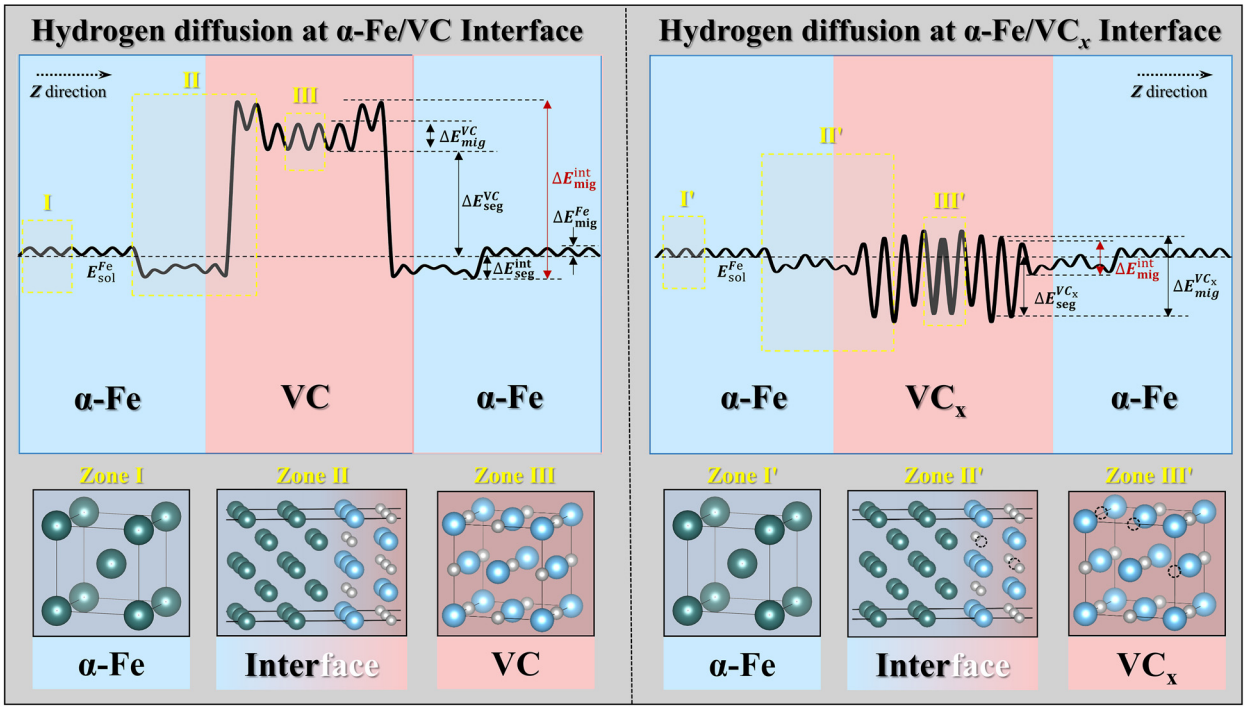


Fig. 9 Schematic of diffusion near the α-Fe/VC interface without and with C vacancies.

near the interface is able to trap hydrogen, but these traps are reversible that do not effectively stabilize hydrogen atoms. Therefore, they cannot substantially mitigate hydrogen embrittlement in steel. Additionally, hydrogen faces significant difficulty in diffusing across the interface into the VC layer, where the hydrogen trapping sites are insufficient to trap hydrogen atoms effectively. In contrast, when C vacancies are present at the interface and a grid of connected C vacancies exists within the VC layer, the hydrogen atom can diffuse sequentially through the channel to the interior of the carbide, and effective hydrogen trapping occurs within the carbide. These sites function as irreversible hydrogen traps, maximizing the hydrogen trapping capacity of VC precipitates to reduce the hydrogen embrittlement susceptibility of steel.

Notably, the vacancy formation energy of the first layer of C vacancy near the interface is only −0.03 eV, while for the third layer of C vacancy, it is −0.47 eV. Although both formation energies are negative, indicating that vacancies can form, C vacancies inside VC are more easily generated than those at the interface, suggesting that the concentration of C vacancies inside VC should be higher than at the interface. This is consistent with the higher hydrogen concentration at the carbide center shown in the APT results.[30,68] Thus, exploring methods to increase the number of C vacancies at the α-Fe/VC interface would be beneficial, since it would increase the effective trapping sites in VC and enhance the likelihood of hydrogen diffusion into the interior of VC, maximizing the hydrogen trapping potential of VC. Furthermore, the connected C vacancies play a key role in facilitating hydrogen diffusion into the VC interior. This configuration allows VC to trap hydrogen atoms effectively. VC in steel commonly exists as the sub-stoichiometric carbide $V_4C_3$, which contains a substantial number of C vacancies.[69] Maximizing the utilization of these C vacancies would significantly reduce the hydrogen embrittlement susceptibility of steel. Based on previous literature studies, two primary strategies can be employed to achieve this. The first involves alloy composition design. The formation of complex carbides such as (V, Mo)C, (V, Nb)C, and (Ti, Mo)C can effectively promote hydrogen entry into the carbide lattice.[30,66,70] The second strategy concerns optimizing the heat treatment process. Specifically, elevating the heat treatment temperature and prolonging the soak time can promote the generation of carbon vacancies, thereby increasing the effective vacancy concentration within the precipitated phase.[29,71]

## 4. Conclusions

We have systematically investigated the role of carbon vacancies in hydrogen trapping and diffusion at the α-Fe/VC interface using first-principles calculations. In the absence of carbon vacancies, hydrogen atoms are confined to reversible trapping sites within the Fe layer near the interface, with an activation energy of 24.5–34.7 kJ mol$^{-1}$, and cannot penetrate the VC layer. The introduction of interfacial carbon vacancies, however, significantly reduces the diffusion barrier across the interface, enabling hydrogen atoms to be trapped irreversibly at these sites. Furthermore, hydrogen migrates preferentially along the *xy*-plane *via* interconnected carbon vacancy networks, sequentially occupying vacancies and diffusing into the VC

 

interior. Both interfacial (67.5 kJ $mol^{-1}$) and internal carbide vacancies (82.2–83.9 kJ $mol^{-1}$) serve as irreversible hydrogen traps, with calculated activation energies consistent with experimental TDS data. Our work highlights that engineering interfacial carbon vacancies and ensuring connectivity within the vacancy network are key strategies to enhance the hydrogen trapping capacity of VC precipitates, thereby effectively mitigating hydrogen embrittlement in advanced steels.

## Author contributions

Linxian Li: writing – review & editing, writing – original draft, visualization, validation, investigation, and formal analysis. Huifang Lan: writing – review & editing, supervision, data curation, and conceptualization. Shuai Tang: writing – conceptualization, review & editing, software, resources, project administration, methodology, funding acquisition, and supervision. Fengliang Tan: resources and data curation. Qing Peng: writing – review & editing, resources, methodology, and funding acquisition. Zhenyu Liu: writing – review & editing and supervision. Guodong Wang: writing – review & editing and supervision.

## Conflicts of interest

There are no conflicts to declare.

## Data availability

The data are available from the corresponding author on reasonable request.

## Acknowledgements

S. T. gratefully acknowledges the financial support from the National Science and Technology Major Project (Grant No. 2025ZD0611901) and the National Natural Science Foundation of China (Grant No. 52175293 and 51774083). Q. P. would like to acknowledge the support provided by the National Natural Science Foundation of China (Grant No. 12272378) and the Open Research Fund of the State Key Laboratory of Rolling and Automation, Northeastern University (2022RALKFKT006).

## References

1 M. Omiya, S. Arakawa, Z. Yao, M. Muramatsu, S. Nishi, K. Takada, M. Murata, K. Okato, K. Ogawa, K. Oide, T. Kobayashi, J. Han and K. Terada, *Eng. Fract. Mech.*, 2022, **271**, 108573, DOI: 10.1016/j.engfracmech.2022.108573.
2 F. Yaghoobi, R. Jamaati and H. J. Aval, *Mater. Chem. Phys.*, 2022, **281**, 125909, DOI: 10.1016/j.matchemphys.2022.125909.
3 H. Li, J. Venezuela, Q. Zhou, V. Luzin, M. Yan, Z. Shi, R. Knibbe, M. Zhang, F. Dong, M. S. Dargusch and A. Atrens, *Mater. Today Commun.*, 2021, **26**, 101887, DOI: 10.1016/j.mtcomm.2020.101887.
4 P. Gong, A. Turk, J. Nutter, F. Yu, B. Wynne and P. Rivera-Diaz-del-Castillo, and W Mark Rainforth, *Acta Mater.*, 2022, **223**, 117488, DOI: 10.1016/j.actamat.2021.117488.
5 M. Rossini, P. R. Spena, L. Cortese, P. Matteis and D. Firrao, *Mater. Sci. Eng., A*, 2015, **628**, 288–296, DOI: 10.1016/j.msea.2015.01.037.
6 H. K. D. H. Bhadeshia, *ISIJ Int.*, 2016, **56**, 24–36, DOI: 10.2355/isijinternational.isijint-2015-430.
7 M. Koyama, E. Akiyama, Y. Lee, D. Raabe and K. Tsuzaki, *Int. J. Hydrog. Energy*, 2017, **42**, 12706–12723, DOI: 10.1016/j.ijhydene.2017.02.214.
8 N. Takano, *Mater. Sci. Eng. A*, 2008, **483**, 336–339, DOI: 10.1016/j.msea.2006.08.144.
9 J. Song and W. A. Curtin, *Nat. Mater.*, 2013, **12**, 145–151, DOI: 10.1038/nmat3479.
10 D. H. Lassila and H. K. Birnbaum, *Acta Metall.*, 1986, **34**, 1237–1243, DOI: 10.1016/0001-6160(86)90010-6.
11 F. G. Wei and K. Tsuzaki, *Metall. Mater. Trans. A*, 2006, **37**, 331–353, DOI: 10.1016/10.1007/s11661-006-0004-3.
12 F. Wei, T. Hara and K. Tsuzaki, *Adv. Steels*, 2011, 87–92, DOI: 10.1007/978-3-642-17665-4_11.
13 E. Wallaert, T. Depover, M. Arafin and K. Verbeken, *Metall. Mater. Trans. A*, 2014, **45**, 2412–2420, DOI: 10.1007/s11661-013-2181-1.
14 A. Nagao, M. L. Martin, M. Dadfarnia, P. Sofronis and I. M. Robertson, *Acta Mater.*, 2014, **74**, 244–254, DOI: 10.1016/j.actamat.2014.04.051.
15 R. Nazarov, T. Hickel, J. Neugebauer, M. Mrovec, C. Elsässer and D. Di Stefano, *Phys. Rev. B*, 2016, **93**, 184108, DOI: 10.1103/PhysRevB.93.184108.
16 H. Liu, H. Zhou, G. Luo and P. Zheng, *J. Nucl. Mater.*, 2021, **554**, 153071, DOI: 10.1016/j.jnucmat.2021.153071.
17 T. Depover and K. Verbeken, *Mater. Sci. Eng., A*, 2016, **675**, 299–313, DOI: 10.1016/j.msea.2016.08.053.
18 H. J. Seo, J. N. Kim, J. W. Jo and C. S. Lee, *Int. J. Hydrog. Energy*, 2021, **46**, 19670–19681, DOI: 10.1016/j.ijhydene.2021.03.109.
19 Y. Li, X. Zhang and T. Wu, *Int. J. Hydrog. Energy*, 2021, **46**, 22030–22039, DOI: 10.1016/j.ijhydene.2021.04.056.
20 L. Li, B. Song, Z. Cai, Z. Liu and X. Cui, *Mater. Sci. Eng., A*, 2019, **742**, 712–721, DOI: 10.1016/j.msea.2018.09.048.
21 X. Yu, G. B. Thompson and C. R. Weinberger, *J. Eur. Ceram. Soc.*, 2015, **35**, 95–103, DOI: 10.1016/j.jeurceramsoc.2014.08.021.
22 W. S. Williams, *Mater. Sci. Eng. A*, 1988, **105–106**, 1–10, DOI: 10.1016/0025-5416(88)90474-0.
23 S. Tang, L. Li, Q. Peng and H. Yan, *Phys. Chem. Chem. Phys.*, 2022, **24**, 20400–20408, DOI: 10.1039/D2CP02425J.
24 K. Kawakami and T. Matsumiya, *ISIJ Int.*, 2012, **52**, 1693–1697, DOI: 10.2355/isijinternational.52.1693.
25 S. Echeverri Restrepo, D. Di Stefano and M. Mrovec, *Int. J. Hydrog. Energy*, 2020, **45**, 2382–2389, DOI: 10.1016/j.ijhydene.2019.11.102.
26 S. Yamasaki and H. K. D. H. Bhadeshia, *Proc. R. Soc. London, Ser. A*, 2006, **462**, 2315–2330, DOI: 10.1098/rspa.2006.1688.
27 R. Shi, Y. Wang, S. Lu, S. Liu, Y. Tu, S. Yang, K. Gao, X. Yang and X. Pang, *Mater. Sci. Eng., A*, 2023, **874**, 145084, DOI: 10.1016/j.msea.2023.145084.

28 T. Boot, A. Suresh Kumar, S. Eswara, P. Kömmelt, A. Böttger and V. Popovich, *J. Mater. Sci.*, 2024, **59**, 7873–7892, DOI: 10.1007/s10853-024-09611-7.
29 J. Takahashi, K. Kawakami and Y. Kobayashi, *Acta Mater.*, 2018, **153**, 193–204, DOI: 10.1016/j.actamat.2018.05.003.
30 Y. Chen, D. Haley, S. S. A. Gerstl, A. J. London, F. Sweeney, R. A. Wepf, W. M. Rainforth, P. A. J. Bagot and M. P. Moody, *Science*, 2017, **355**, 1196–1199, DOI: 10.1126/science.aal2418.
31 L. Vandewalle, T. Depover and K. Verbeken, *Int. J. Hydrog. Energy*, 2023, **48**, 32158–32168, DOI: 10.1016/j.ijhydene.2023.04.348.
32 J. Nguyen, N. Glandut, C. Jaoul and P. Lefort, *Int. J. Hydrog. Energy*, 2015, **40**, 8562–8570, DOI: 10.1016/j.ijhydene.2015.05.009.
33 Y. Ma, Y. Shi and H. Wang, *Int. J. Hydrog. Energy*, 2020, **45**, 27941–27949, DOI: 10.1016/j.ijhydene.2020.07.123.
34 B. Zhang, J. Su and M. Wang, *Acta Mater.*, 2021, **208**, 116744, DOI: 10.1016/j.actamat.2021.116744.
35 S. Sagar, M. H. F. Sluiter and P. Dey, *Int. J. Hydrog. Energy*, 2024, **50**, 211–223, DOI: 10.1016/j.ijhydene.2023.09.222.
36 G. Kresse and J. Furthmüller, *Comput. Mater. Sci.*, 1996, **6**, 15–50, DOI: 10.1016/0927-0256(96)00008-0.
37 J. Enkovaara, C. Rostgaard, J. J. Mortensen and J. Chen, *J. Phys.: Condens. Matter*, 2010, **22**, 253202, DOI: 10.1088/0953-8984/22/25/253202.
38 J. P. Perdew, K. Burke and M. Ernzerhof, *Phys. Rev. Lett.*, 1996, **77**, 3865–3868, DOI: 10.1103/PhysRevLett.77.3865.
39 J. P. Perdew, J. A. Chevary and S. H. Vosko, *Phys. Rev. B: Condens. Matter Mater. Phys.*, 1993, **48**, 4978, DOI: 10.1103/PhysRevB.48.4978.2.
40 J. Takahashi, K. Kawakami and T. Tarui, *Scr. Mater.*, 2012, **67**, 213–216, DOI: 10.1016/j.scriptamat.2012.04.022.
41 T. Epicier, D. Acevedo and M. Perez, *Philos. Mag.*, 2008, **88**, 31–45, DOI: 10.1080/14786430701753816.
42 Z. Nana, R. Congcong, Z. Jiajing, W. Yuting, C. Zhen and Z. Lisheng, *Mater. Today Commun.*, 2024, **38**, 107592, DOI: 10.1016/j.mtcomm.2023.107592.
43 L. Chen, Y. Li, Z. Zhao, Q. Zheng, D. Yi, X. Li, J. Peng and L. Sun, *Chem. Phys.*, 2021, **547**, 111193, DOI: 10.1016/j.chemphys.2021.111193.
44 D. J. Chadi, *Phys. Rev. B: Condens. Matter Mater. Phys.*, 1977, **16**, 1746–1747, DOI: 10.1016/10.1103/PhysRevB.16.1746.
45 G. Henkelman and H. Jónsson, *J. Chem. Phys.*, 1999, **111**, 7010–7022, DOI: 10.1063/1.480097.
46 K. Momma and F. Izumi, *J. Appl. Crystallogr.*, 2011, **44**, 1272–1276, DOI: 10.1107/S0021889811038970.
47 L. Li, H. Lan, S. Tang, H. Yan, F. Tan, S. van der Zwaag, Q. Peng, Z. Liu and G. Wang, *Int. J. Hydrog. Energy*, 2024, **91**, 611–617, DOI: 10.1016/j.ijhydene.2024.10.150.
48 S. Tang, L. Li, H. Yan, J. Jin, Q. Peng, M. Cai, J. Li, Z. Liu and G. Wang, *Nucl. Mater. Energy*, 2023, **36**, 101504, DOI: 10.1016/j.nme.2023.101504.
49 W. A. Counts, C. Wolverton and R. Gibala, *Acta Mater.*, 2010, **58**, 4730–4741, DOI: 10.1016/j.actamat.2010.05.010.
50 E. A. Carter and D. E. Jiang, *Phys. Rev. B: Condens. Matter Mater. Phys.*, 2004, **70**, 64102, DOI: 10.1103/PhysRevB.70.064102.
51 X. L. Xiong, H. X. Ma, L. N. Zhang, K. K. Song, Y. Yan, P. Qian and Y. J. Su, *Comput. Mater. Sci.*, 2023, **216**, 111854, DOI: 10.1016/j.commatsci.2022.111854.
52 W. Y. Choo and J. Y. Lee, *Metall. Trans. A*, 1982, **13**, 135–140, DOI: 10.1007/BF02642424.
53 Y. Lin, H. L. Yi, Z. Y. Chang, H. Lin and H. Yen, *Front. Mater.*, 2021, 7, DOI: 10.3389/fmats.2020.611390.
54 E. Wallaert, T. Depover, M. Arafin and K. Verbeken, *Metall. Mater. Trans. A*, 2014, **45**, 2412–2420, DOI: 10.1007/s11661-013-2181-1.
55 D. Pérez Escobar, E. Wallaert, L. Duprez, A. Atrens and K. Verbeken, *Met. Mater. Int.*, 2013, **19**, 741–748, DOI: 10.1007/s12540-013-4013-7.
56 V. Ortolland, F. Martin, Q. Auzoux and K. Wolski, *Int. J. Hydrog. Energy*, 2024, **67**, 577–591, DOI: 10.1016/j.ijhydene.2024.02.264.
57 C. Hai, Y. Zhu, E. Fan, C. Du, X. Cheng and X. Li, *Corros. Sci.*, 2023, **218**, 111164, DOI: 10.1016/j.corsci.2023.111164.
58 Y. Zhou, W. Wu and J. Li, *Int. J. Hydrog. Energy*, 2024, **58**, 1372–1385, DOI: 10.1016/j.ijhydene.2024.01.270.
59 T. Tan, L. Sun, Y. Cheng, J. Huang and H. Wang, *Met. Mater. Int.*, 2025, **31**, 666–675, DOI: 10.1007/s12540-024-01769-8.
60 Y. Sun, J. Chen and J. Liu, *J. Iron Steel Res. Int.*, 2015, **22**, 961–968, DOI: 10.1016/S1006-706X(15)30097-2.
61 A. K. Belyaev, A. M. Polyanskiy, V. A. Polyanskiy, C. Sommitsch and Y. A. Yakovlev, *Int. J. Hydrog. Energy*, 2016, **41**, 8627–8634, DOI: 10.1016/j.ijhydene.2016.03.198.
62 Y. Sun, J. Chen and J. Liu, *Mater. Sci. Eng., A*, 2015, **625**, 89–97, DOI: 10.1016/j.msea.2014.12.013.
63 T. Michler and M. P. Balogh, *Int. J. Hydrog. Energy*, 2010, **35**, 9746–9754, DOI: 10.1016/j.ijhydene.2010.06.071.
64 Y. Chen, C. Huang, P. Liu, H. Yen, R. Niu, P. Burr, K. L. Moore, E. Martínez-Pañeda, A. Atrens and J. M. Cairney, *Int. J. Hydrog. Energy*, 2025, **136**, 789–821, DOI: 10.1016/j.ijhydene.2024.04.076.
65 H. Asahi, D. Hirakami and S. Yamasaki, *ISIJ Int.*, 2003, **43**, 527–533, DOI: 10.2355/isijinternational.43.527.
66 M. Moshtaghi, E. Maawad, A. Bendo, A. Krause, J. Todt, J. Keckes and M. Safyari, *Mater. Des.*, 2023, **234**, 112323, DOI: 10.1016/j.matdes.2023.112323.
67 E. Van den Eeckhout, T. Depover and K. Verbeken, *Metals*, 2018, **8**, 779, DOI: 10.3390/met8100779.
68 S. Samanta, S. Gangavarapu, B. Jayabalan, S. K. Makineni, M. Dutta and S. B. Singh, *Scr. Mater.*, 2023, **234**, 115537, DOI: 10.1016/j.scriptamat.2023.115537.
69 G. R. Speich and W. C. Leslie, *Metall. Trans.*, 1972, **3**, 1043–1054, DOI: 10.1007/BF02642436.
70 P. Y. Liu, B. Zhang, R. Niu, S. L. Lu, C. Huang, M. Wang, F. Tian, Y. Mao, T. Li, P. A. Burr, H. Lu, A. Guo, H. W. Yen, J. M. Cairney, H. Chen and Y. S. Chen, *Nat. Commun.*, 2024, **15**, 724, DOI: 10.1038/s41467-024-45017-4.
71 Z. Zhu, D. Yang, S. Tang, D. Liu and H. Yi, *Mater. Charact.*, 2025, **219**, 114604, DOI: 10.1016/j.matchar.2024.114604.

 